Published in Journal of Applied Thermal Engineering (2006)
This is accepted postprint (author's version)
Archived in Dspace@nitr http://dspace.nitrkl.ac.in/dspace

Mathematical Modeling of the Working Cycle of Oil Injected Rotary Twin Screw Compressor

***N.Seshaiah., Subrata Kr. Ghosh., R.K. Sahoo., Sunil Kr. Sarangi**
Cryogenics and Gas dynamics Laboratory, Mechanical Engineering Department, National Institute of Technology, Rourkela -769008, Orissa State, India.

Abstract

Oil injected twin-screw air and gas compressors are widely used for medium pressure applications in many industries. Low cost air compressors can be adopted for compression of helium and special gases, leading to significant cost saving. Mathematical analysis of oil injected twin-screw compressor is carried out on the basis of the laws of perfect gas and standard thermodynamic relations. Heat transfer coefficient required for computer simulation is experimentally obtained and used in performance prediction, when the working medium being air or helium. A mathematical model has been developed for calculating the compressor performance and for validating the results with experimental data. The flow coefficients required for numerical simulation to calculate leakage flow rates are obtained from efficiency verses clearance curves. Effect of some of the compressor operating and design parameters on power and volumetric efficiencies have been analyzed and presented.

(**Key words**: screw compressor, oil injection, heat transfer coefficient, leakage, flow coefficients)

*Corresponding author: Tel: 91-9437109766; fax: 91-661-2462999
E- Mail address: seshuet@yahoo.com

Nomenclature

A Heat transfer area (m^2)

A_c Leakage clearance area (m^2)

A_e Experimental adiabatic power required for the compressor (W)

A_f Cross sectional area of female rotor groove (m^2)

A_m Cross sectional area of male rotor groove (m^2)

A_s Input power to the compressor (W)

A_t Theoretical adiabatic power of the compressor (W)

a Clearance between lobe tip and housing(m)

C Flow coefficient (dimensionless)

C_l Specific heat of lubricating oil (J/kg K)

C_p Specific heat of gas at constant pressure (J/kg K)

C_v Specific heat of gas at constant volume (J/kg K)

D Rotor diameter (m)

e Interlobe clearance (m)

h Heat transfer coefficient between gas and oil ($W/m^2 K$)

i Specific enthalpy (kJ/kg)

H_g Enthalpy of gas (J)

k Ratio of specific heats (dimensionless)

M_g Mass of gas in the working space (kg)

M_l Mass of oil in the working space (kg)

M_{t1} Theoretical gas mass in a pair of male and female cavities at the end of suction process (kg)

M_{il} Interlobe leakage mass leaked into the suction cavity during previous compression process (kg)

m Leakage mass flow rate through flow path (kg/s)

m_t Theoretical mass flow rate in to the suction chamber at suction condition (kg/s)

m_e Actual discharged gas mass rate (kg/s)

m_b Leakage mass flow rate through blowhole (kg/s)

m_d Leakage gas mass flow rate through clearance between rotor end and casing wall (kg/s)

m_{il} Leakage gas mass flow rate through interlobe clearance (kg/s)

m_{lr} Leakage mass flow rate of oil through rotor tip housing clearance (kg/s)

m_{gl} Net gas mass leakage rate from a pair of grooves during compression process (kg/s)

m_{gt} Total gas mass leakage rate per second (kg/s)

m_{dt} Theoretical discharged gas mass rate (kg/s)

N Rotational speed of rotor (RPS)

P Pressure in the working space (N/m^2)

P_d Discharge pressure (N/m^2)

P_s Suction pressure (N/m^2)

Q Heat transferred between gas and oil (J)

q Leakage volume flow rate through flow path (m^3/s)

R Gas constant (J/kg-K)

R_m Modified gas constant of oil gas mixture (J/kg-K)

r Pressure ratio (dimensionless)

S Sealing line length along the rotor (m)

T Temperature (K)

t Time (s)

T_1 Temperature of gas at the end of suction process (K)

T_g Temperature of gas in the working space (K)

T_l Temperature of oil in the working space (K)

T_{oil} Mean temperature of leaked oil in the suction cavity (K)

T_s Inlet gas temperature (K)

t_s Time required for suction process (s)

U Internal energy (J)

V Volume of the working space (m^3)

V_t Rotor tip speed (m/s)

V_1 Inducted gas volume at inlet condition (m^3)

V_2 Leakage gas volume at inlet pressure (m^3)

V_{t1} Geometrical volume of one pair of male and female cavities (working chamber) (m^3)

W Gas work (J)

w_t Lobe tip width (m)

Greek Symbols

η_v volumetric efficiency (dimensionless)

η_a adiabatic efficiency (dimensionless)

η_{tv} Theoretical volumetric efficiency (dimensionless)

η_{ev} Experimental volumetric efficiency (dimensionless)

η_{ta} Theoretical adiabatic efficiency (dimensionless)

η_{ea} Experimental adiabatic efficiency (dimensionless)

φ Oil to gas mass ratio (dimensionless)

θ Rotor rotational angle (degrees)

Φ Male rotor wrap angle (degrees)

β Modified adiabatic index (dimensionless)

μ Dynamic viscosity of oil (N.s/m^2)

ρ Density (kg/m^3)

Γ Time for compression process (s)

τ Cycle time of compressor (s)

Subscripts

1 Upstream

2 Downstream

b Beyond flow path

f Female rotor

g Gas

i Gas or oil going in to the working space

l Oil

m Male rotor

o Gas or oil going out of the working space

1. Introduction

The screw compressor is a positive displacement machine that uses a pair of intermeshing rotors housed in a suitable casing to produce compression. Screw compressors are capable of high-speed operation over a wide range of operating pressures. In a screw machines, oil is deliberately injected into the compression chamber to improve and to provide sealing, lubrication, corrosion resistance and cooling effect. Rotary dual screw compressors are widely used in industry for air and gas compression and for refrigeration applications. They are particularly suitable for compression of air and helium used in small and intermediate size cryogenic

refrigerators and liquefiers. A computerized method for generation of rotor profiles and analysis and performance has been suggested by Singh *et al* [1, 2]. Due to the high cost of energy, particularly in India, it is necessary that all machines operate efficiently. This can be achieved only when machine performance is well understood and is predictable. Unlike other compressors, the mechanism of gas compression in an oil injected screw compressor is extremely complex. It is difficult to estimate the compressor performance analytically. On the other hand, experimental studies are prohibitively expensive because a new rotor needs to be fabricated using expensive machining techniques for every change in rotor geometry.

2. Modeling of Compressor Cycle

Analysis of volumetric and power efficiencies is essential to estimate the suitability of a compressor for a particular application. The main objective of the present performance analysis is to develop a numerical model to ascertain the suitability of a commercially available air compressor for different gas compression applications. Efficiency of any compressor depends on the processes involved in the working cycle. Major processes of screw compressor are suction, compression and discharge. Analysis of these individual processes is essential to model the compressor performance.

2.1. Suction Process

Volumetric efficiency of the compressor greatly depends on the amount of gas mass inducted into the suction cavity during suction process. This, in turn, depends on the temperature of the cavity walls at steady state. Analysis of the suction process gives the average temperature of the gas in the suction cavity at the end of suction process. Model of the working chamber during suction process is shown in Fig 1. Since the

pressure and temperature fluctuations during suction process are generally small, the following quantities are assumed to be constant during the suction process.

- Inlet velocities of gas and oil
- Inlet temperature of gas and oil
- Pressure drop across the inlet port
- Rate of heat flow from gas to oil (or from oil to gas)

The quantity of gas mass inducted into the suction cavities depends on the temperatures of inlet gas and the cavity walls. During the suction process the cavity wall temperature is higher than the inducted gas temperature because of the heat flow from the compressed gas during the compression process. The cavity wall is covered with a film of lubricating oil which leaks from the adjoining compression space when the oil is injected. The amount of heat transferred from the hot suction cavity wall (lubricating oil film) to the inducted gas during suction process can be estimated by the expression

$$Q = M_1 C_p (T_1 - T_s) \tag{1}$$

If the temperature rise of the inducted gas is small compared to the temperature difference between the lubricating oil film and the inducted gas, the heat transfer between the leaked oil and inducted gas may be written as below.

$$Q = hA(T_{oil} - T_s)t_s \tag{2}$$

Under ideal conditions, the heat lost by the oil film must be equal to heat gained by the fresh gas mass. From equations (1) and (2), the mean temperature of inducted gas at the end of suction process can be obtained as:

$$T_1 = \frac{hA(T_{oil} - T_s)t_s}{M_1 c_p} + T_s \tag{3}$$

The amount of gas mass inducted into the geometrical volume at suction condition (P_s,T_s) is

$$M_{ts} = \frac{P_s V_{t1}}{R T_s} \tag{4}$$

V_{t1}, the geometrical volume of a pair of male and female rotor cavities is defined [3] as below

$$V_{t1} = (A_m + A_f)L$$

A_m, and A_f being the cross sectional areas of the male and female cavities respectively and L the rotor length.

The gas mass in the suction cavity at condition (P_s,T_1) can be estimated by the expression

$$M_{t1} = M_{ts} \frac{T_s}{T_1} \tag{5}$$

This gas mass is the sum of fresh charge inducted (M_1) and the mass leaked through interlobe clearance (M_{il}):

$$M_{t1} = M_1 + M_{il} \tag{6}$$

Eliminating the total mass M_{t1} between equations (5) and (6), the fresh gas mass inducted during suction process is obtained as below.

$$M_1 = M_{ts} \frac{T_s}{T_1} - M_{il} \tag{7}$$

Substituting this value of M1 value in equation (3), the following quadratic equation is obtained in terms of the gas temperature T_1.

$$-c_p M_{il} T_1^{\,2} + T_1 \left[c_p M_{t1} T_s + c_p M_{il} T_s - hA(T_{oil} - T_s)t_s \right] - c_p M_{t1} T_s^{\,2} = 0 \tag{8}$$

2.2. Compression and Discharge Process

Both the compression and the discharge processes are unsteady processes. Thermodynamic properties of the gas and oil vary continuously during compression process. The gas in the working chamber is compressed to a high pressure by the

rotational movement of the rotors. To simplify the analysis, it is assumed that the oil and gas are separate fluids, and only heat is exchanged between them. The discharge port is so located that the cavities connect to the discharge port when the pressure in the working chamber reaches the designed discharge pressure and discharge continues till the male rotor lobe completely disengage from female rotor groove.

The following factors are taken into account in the model:

1. volume change due to rotor rotation,
2. mass and enthalpy flows of gas entering or leaving the working space through discharge port and leakage paths,
3. mass and enthalpy flows of oil, entering or leaving the working space through discharge port and leakage paths,
4. heat exchange between gas and oil.

To simplify the calculations, the following assumptions are made:

- Gas and oil temperatures are homogeneous at any instant in the working space.
- Gas and oil never change phase.
- Pressure is uniform throughout the working space at any stage.
- The working gas is an ideal gas.
- Oil is an incompressible fluid.
- Heat exchange between gas and oil is in proportion to the temperature difference between them.
- A pressure fluctuation across the discharge port is negligible.

Fujiwara and Osada [4] derived the fundamental equations based on standard thermodynamic laws and the laws of perfect gas. The following equations are derived with some modifications and other details are introduced as needed.

The first law of thermodynamics for unsteady flow of gas through the working chamber can be expressed as

$$\frac{dE_v}{dt} = m_{gi} i_{gi} + \frac{dQ}{dt} - m_{go} i_{go} - \frac{dW}{dt} \tag{9}$$

E_v is the sum of internal, potential and kinetic energies. Assuming the potential and kinetic energies of gas to be negligible, from the above equation the change in internal energy in time dt can be computed as:

$$dU_g = dQ - dW + dH_g \tag{10}$$

Change in internal energy can also be expressed as a function of mass and temperature change and defined as below:

$$dU_g = c_V M_g dT_g + c_V T_g dM_g \tag{11}$$

The change of enthalpy due to leakage can be expressed as:

$$dH_g = c_p T_{gb} dM_{gi} - c_p T_g dM_{go} \tag{12}$$

The gas work may be expressed in terms of geometrical volume change, and oil volume change due to leakage. Since the oil is an incompressible fluid, the gas work is expressed as:

$$dW = PdV + Pq_{lo} dt - P_{bi} q_{li} dt \tag{13}$$

Heat exchange between the gas and the oil in time dt is assumed to follow the Newton's law of cooling and is expressed as:

$$dQ = -hA(T_g - T_l)dt \tag{14}$$

Substituting equations (11), (12), (13) and (14) in equation (10), and rearranging, the rate of change of working gas temperature is obtained.

$$\frac{dT_g}{dt} = [-\frac{(k-1)T_g}{V_g}(\frac{dV}{dt} - \frac{P_b}{P} q_{li} + q_{l0}) + \frac{m_{gi}}{M_g}(kT_{gb} - T_g) - \frac{m_{go}}{M_g}(k-1)T_g - \frac{hA}{c_v M_g}(T_g - T_l)] \tag{15}$$

The first term on the right-hand side of the above equation relates to the change in volume including the leakage rate of oil. The second and third terms represent the effect

of gas leakage into and out of the compressor cavity respectively. The last term is derived from the heat transfer from gas to the oil.

The rate of change of net gas volume of the working chamber [4] can be written as below

$$\frac{dV_g}{dt} = \frac{dV}{dt} - q_{li} + q_{lo} \tag{16}$$

The rate of change of gas mass due to internal leakage is given by the expression

$$\frac{dM_g}{dt} = m_{gi} - m_{go} \tag{17}$$

The equation of state of perfect gas may be written as follows

$$PV_g = M_g R T_g$$

The differential form of the above equation can be written as follows

$$\frac{dP}{dt} = \frac{1}{V_g}\left[- P\frac{dV_g}{dt} + RT_g\frac{dM_g}{dt} + RM_g\frac{dT_g}{dt}\right] \tag{18}$$

Substituting equations (15, (16), and (17) in equation (18), the rate of change of pressure is obtained as follows.

$$\begin{aligned}\frac{dP}{dt} = \frac{1}{V_g}[& -kP(\frac{dV}{dT} + q_{l0}) + (kP_b - P_b + P)q_{li} + k\frac{T_{gb}PV_g}{T_g M_g}m_{gi} \\ & - k\frac{PV_g}{M_g}m_{g0} - \frac{PV_g hA}{c_v M_g T_g}(T_g - T_l)]\end{aligned} \tag{19}$$

The rate of change of oil temperature is obtained from energy balance in terms of leakage oil temperature and heat transferred from the gas. The increase of oil temperature in the working chambers is due to heat gained from the leakage oil (which is at higher temperature) and the heat gained from the gas under compression.

Assuming the potential and kinetic energies to be negligible, the enthalpy change of oil in the working chamber can be expressed as follows.

$$dH_l = dW_l + dQ + dJ_l \tag{20}$$

where, dJ_1 is the heat lost by the leaked oil.

The enthalpy change of oil in time dt may be expressed as

$$dH_l = M_l c_l dT_l \tag{21}$$

The work done by the oil is zero (i.e dW=0), since oil is an incompressible fluid

The heat gained by the oil in time dt is given by the expression

$$dQ = hA(T_g - T_l)dt \tag{22}$$

The oil leakage in to the working chamber is at higher temperature than the oil in the cavity. The energy lost by leaked oil is given by the expression

$$dJ_l = m_{li} c_l (T_{lb} - T_l)dt \tag{23}$$

Substituting equations (21), (22), (23) in equation (20), the rate of change of oil temperature is obtained as follows:

$$\frac{dT_l}{dt} = (T_{lb} - T_l)\frac{m_{li}}{M_l} + \frac{hA}{M_l c_l}(T_g - T_l) \tag{24}$$

The rate of change of oil mass in the working chamber due to leakage as follows

$$\frac{dM_l}{dt} = m_{li} - m_{lo} \tag{25}$$

2.3 Leakage calculation of gas and oil

Leakage is a major concern in screw compressors. The major leakage paths identified during compression process are leakage through interlobe clearance, through blowhole, rotor tip-housing clearance and clearance between rotor discharge end and casing wall [5, 6, 7]. Leakage mass through interlobe clearance will go directly into the suction chambers. Except at the lobe tip clearance, leakage gas and oil are uniformly mixed and the flow is isolated from any heat exchange with their surroundings while maintaining thermal equilibrium. In this study, the leakage rate is assumed to follow the well-known equation for flow through a convergent nozzle [8, 9].

$$m = (m_g + m_l) = \frac{CA_c P_1}{\sqrt{T_1}} \sqrt{\frac{2\beta(r^{\frac{2}{\beta}} - r^{\frac{\beta+1}{\beta}})}{(\beta-1)R_m}} \quad \text{for} \quad r > \left(\frac{2}{\beta+1}\right)^{\frac{\beta}{\beta-1}} \tag{26}$$

and

$$m = \frac{CA_c P_1}{\sqrt{T_1}} \sqrt{\frac{\beta\left(\frac{2}{\beta-1}\right)^{\frac{\beta+1}{\beta-1}}}{R_m}} \quad \text{for} \quad r \le \left(\frac{2}{\beta+1}\right)^{\frac{\beta}{\beta-1}}$$

where, $r = \frac{P_2}{P_1}$, P_1 & P_2 being upstream and down stream pressures respectively.

Due to the presence of oil, exact properties of oil-gas mixture are not known. However, the properties are calculated based on well justifiable assumptions and compared with experimental data. By comparison with laboratory tests, the following assumptions for different types of leakage paths have been shown to be the most appropriate [5].

(1) The gas/oil mixture in all leakage paths is homogeneous.

(2) The gas/oil mixture ratio is same in all leakage paths except at the lobe tip clearance and equal to the mixture ratio passing through discharge port.

The apparent ratio of specific heats of oil and gas mixture is calculated from reference [4]

$$\beta = \frac{c_p + \varphi c_l}{c_v + \varphi c_l} \tag{27}$$

The modified gas constant of the mixture is also calculated using reference [4]

$$R_m = \frac{R}{1+\varphi} \tag{28}$$

The mass ratio of oil to gas in the working chambers as well as through all leakage paths is homogeneous and equal to the mixture ratio in the working volume [5] and is expressed as below:

$$\varphi = \frac{M_l}{M_g} = \frac{m_l}{m_g} \tag{29}$$

The Average leakage area is determined by multiplying sealing line length with an average gap (clearance) for each type of leakage. Normally, the average gap/clearance is determined from the actual clearance measurements in the compressor. The discharge or flow coefficients are empirically selected to account in the presence of oil.

At the lobe tip, it is assumed that the clearance fills with the oil due to the action of centrifugal force, and the oil leakage flow is in single phase. The leakage flow rate of oil can be calculated using the equation of incompressible viscous flow through a narrow gap [10] as follows

$$m_{lr} = S\rho_l \left[\frac{V_t a}{2} - \frac{(P_1 - P_2)a^3}{12\mu_l w_t} \right] \tag{30}$$

The leakage gas mass rate into the working chambers is through leading blowhole, and through clearance between discharge end of rotors and casing wall from male and female rotor leading cavities. It can be calculated using the below expression

$$m_{gi} = (m_{gbi} + m_{gdmi} + m_{gdfi})/(1+\varphi) \tag{31}$$

The leakage gas mass going out of the working chambers is through trailing blowhole, interlobe clearance, and through the clearance between lagging cavity end and casing wall, of male and female rotors at discharge end and is expressed as:

$$m_{go} = (m_{gbo} + m_{gilo} + m_{gdmo} + m_{gdfo})/(1+\varphi) \tag{32}$$

Similarly, the leakage rate of oil mass into and out of the working chambers is given by the relations:

$$m_{li} = \varphi m_{gi} + m_{lrmi} + m_{lrfi} \tag{33}$$

$$m_{lo} = \varphi m_{go} + m_{lrmo} + m_{lrfo} \tag{34}$$

Equations (26) to (34) are adequate to calculate the rate of change of gas and oil mass during compression and discharge process.

2.4 Heat Transfer Coefficient

The heat transfer coefficient between gas and oil is essential to estimate the rate of heat transfer between gas and oil. Fujiwara and Osada [4] determined the heat transfer coefficient using experimental performance data. In this study, the same methodology is followed.

The heat transfer coefficient between gas and oil is defined as follows

$$h = \frac{kP_sV_{t1}}{(k-1)At_s}\frac{d\eta_{ev}}{dT_s} \tag{35}$$

Equation (35) relates "h" to the tangent of the η_{ev}-T_s curve. The experimental test setup used to determine heat transfer coefficients and to measure various operating parameters is shown in Fig 2. Applying experimental test data, the change in volumetric efficiency with inlet gas temperature for air and helium are presented in Figures 3 and 4 respectively. The slopes of these lines give the $\frac{d\eta_{ev}}{dT_s}$ value which can be directly substituted in the numerical simulation to find the heat transfer coefficient between gas and oil. The values of $\frac{d\eta_{ev}}{dT_s}$ for air and helium are 0.0026$K^{-1}$and 0.0025K^{-1} respectively (as shown by the straight lines in the figures).The experimental heat transfer coefficients for air and helium are found to be 2.141kW/m^2K, and 1.4656kW/m^2K respectively.

However, there is no exact information available concerning the heat transfer area. Fujiwara and Osada [4] defined the representative heat transfer area between gas and oil as below.

$$A = V_{t1}^{2/3} \tag{36}$$

The time for suction process depends on male rotor rotation speed and defined as follows

$$t_s = \frac{1}{N_m} \tag{37}$$

2.5 Time for compression process

The time for compression and discharge process depends on male wrap angle, male rotor rotational speed and number of male lobes.

The time taken for compression and discharge process in seconds is given by the expression:

$$\Gamma = \frac{1}{N_m}\left(\frac{\Phi}{360} + \frac{1}{n_m}\right) \tag{38}$$

2.6 Total cycle time for suction and compression processes

The time for the entire compression process including suction and compression stages also depends on the male wrap angle, male rotor rotational speed and the number of male lobes.

This cycle time in unites of seconds can be expressed as below.

$$\tau = \frac{1}{N_m}\left(1 + \frac{\Phi}{360} + \frac{1}{n_m}\right) \tag{39}$$

3. Efficiencies

Many standard efficiency definitions exist that qualify the mass flow and power performance characteristics of compressors. Volumetric and power efficiency definitions are taken from standard thermodynamic textbooks and from reference [11].

3.1 Volumetric Efficiency

The theoretical gas mass inducted into any pair of male and female rotor grooves at suction condition can be expressed as

$$M_{ts} = \frac{P_s V_{t1}}{R T_s} \tag{40}$$

The theoretical gas mass inducted into the working chambers at an average temperature of T_1 becomes:

$$M_{t1} = M_{ts} \frac{T_s}{T_1} \tag{41}$$

Thus the theoretical gas mass inducted per second at suction condition comes out as:

$$m_t = M_{t1} N_m n_m \tag{42}$$

The net gas mass leakage rate from a pair of male and female rotor grooves is calculated as given below

$$m_{gl} = m_{gi} - m_{go} \tag{43}$$

The total gas mass leakage rate depends on the number of lobes on the male rotor and its rotational speed. The net leakage rate per second is defined by the relation:

$$m_{gt} = m_{gl} \times N_m \times n_m \tag{44}$$

The theoretical discharged gas mass rate at an average suction condition can be estimated as below.

$$m_{dt} = m_t - m_{gt} \tag{45}$$

Theoretical volumetric efficiency in terms of mass flow rate can be defined as:

$$\eta_{tv} = \frac{m_{dt}}{m_t} \tag{46}$$

The experimental gas mass flow rate will be less than the theoretical inducted mass rate due to imperfect nature of ports, wall friction and other frictional losses apart from leakage loses. Experimental volumetric efficiency may be calculated after measuring the actual discharged mass flow rate.

The experimental volumetric efficiency is defined as:

$$\eta_{ev} = \frac{m_e}{m_t} \tag{47}$$

3.2 Adiabatic Efficiency

The theoretical adiabatic efficiency is defined as below

$$\eta_{ta} = \frac{A_t}{A_s} \tag{48}$$

The theoretical adiabatic power required for the compressor is given by the expression

$$A_t = m_{dt} c_p T_s \left[(\frac{P_d}{P_s})^{\frac{k-1}{k}} - 1 \right] \tag{49}$$

The experimental adiabatic power A_e can be interpreted as the power required to compress the gas adiabatically that produces the actual discharged mass flow rate at the given pressure ratio.

The experimental adiabatic efficiency is defined as:

$$\eta_{ea} = \frac{A_e}{A_s} \tag{50}$$

The experimental power required for the compressor is given by the expression:

$$A_e = m_e c_p T_s \left[(\frac{P_d}{P_s})^{\frac{k-1}{k}} - 1 \right] \tag{51}$$

The actual power consumed by the compressor is inclusive of that consumed by the compressor cooling fan, transmission and electric motor losses, as well as mechanical losses.

4. Outline of computer program

At steady state, all the changes in the compressor working chambers/cavities are related to rotor turning, and the state in a groove varies as function of the rotor turning angle/time. Therefore, if the change in a state of one pair of grooves is calculated, the states in all the grooves can be known. All the equations obtained above are used for suction and discharge process simulation. Inputs required for simulation are listed in the Table 1 and Table 2. For the sake of simplicity, the outlet pressure (discharge pressure) is assumed to be constant. The flow chart for the computer program employed to model the governing equations is shown in Fig 5. Step- by-step calculations start from the end of the suction process.

To calculate the leakage flow rate, the state of the grooves beyond the leakage path must be known a prior, but this information is not available at the beginning of the calculation. Therefore, to start with, the state in the grooves is computed assuming no leakage of gas. Subsequently, the leakage flow is calculated and the state is corrected following the Runge-Kutta procedure. This calculation is iterated until the system converges. Finally volumetric and adiabatic efficiencies are calculated.

5. Error analysis

It has been observed that almost all the error arises from the mass flow rate measurement. Gas volume flow rates are measured with a rotameter and temperature, and pressure are measured with platinum resistance thermometers and pressure transducers respectively. The gas density is determined using an equation of state as a function of pressure, temperature and gas composition. A more realistic expression for the overall uncertainty can be predicted by the root mean square error: [14]

5.1 Uncertainty in determination of volumetric efficiency

The uncertainty in volumetric efficiency determination is calculated as below

$$\Delta\eta_{ev} = \sqrt{\left(\frac{\partial\eta_{ev}}{\partial m_e}\Delta m_e\right)^2 + \left(\frac{\partial\eta_{ev}}{\partial m_t}\Delta m_t\right)^2}$$

Assuming that the uncertainties in the measurement of reference condition and suction temperature and pressure, and thermo-physical properties are negligible, the uncertainty in experimental mass flow rate can be expressed as

$$\Delta m_e = \sqrt{\left(\frac{\partial m_e}{\partial V_m}\Delta V_m\right)^2 + \left(\frac{\partial m_e}{\partial P_s}\Delta P_s\right)^2 + \left(\frac{\partial m_e}{\partial T_s}\Delta T_s\right)^2}$$

The uncertainty associated in measuring the theoretical mass flow rate is in the measurement of theoretical volume of one pair of male and female rotor grooves and that in the speed measurement of the male rotor.

The uncertainty in the theoretical mass flow rate measurement is calculated as follows

$$\Delta m_t = \sqrt{\left(\frac{\partial m_t}{\partial V_{t1}}\Delta V_{t1}\right)^2 + \left(\frac{\partial m_t}{\partial N_m}\Delta N_m\right)^2 + \left(\frac{\partial m_t}{\partial P_s}\Delta P_s\right)^2 + \left(\frac{\partial m_t}{\partial T_s}\Delta T_s\right)^2}$$

5.2 Uncertainty in determination of adiabatic efficiency

The uncertainty in the measurement of adiabatic efficiency is computed as below

$$\Delta\eta_{ea} = \sqrt{\left(\frac{\partial\eta_{ea}}{\partial A_e}\Delta A_e\right)^2 + \left(\frac{\partial\eta_{ea}}{\partial A_s}\Delta A_s\right)^2}$$

The uncertainty in calculation of experimental adiabatic power is expressed as

$$\Delta A_e = \sqrt{\left(\frac{\partial A_e}{\partial m_e}\Delta m_e\right)^2 + \left(\frac{\partial A_e}{\partial T_s}\Delta T_s\right)^2 + \left(\frac{\partial A_e}{\partial P_d}\Delta P_d\right)^2 + \left(\frac{\partial A_e}{\partial P_s}\Delta P_s\right)^2}$$

and the uncertainty associated in measuring the system power is calculated as

$$\Delta A_s = \sqrt{\left(\frac{\partial A_s}{\partial n_e}\Delta n_e\right)^2 + \left(\frac{\partial A_s}{\partial t_e}\Delta t_e\right)^2}$$

One data point from the test facility has been taken from the multiple data of various measurable parameters such as suction and discharge pressure, temperature, RPM of male rotor, time taken for a specified number of revolutions of energy meter, and flow rate measurement. The average value of the samples at same operating conditions is recorded as a data point. The standard deviation of the average value is recorded as a component of uncertainty for that data point. This component represents the observed random effect associated with a particular measurement.

As an example, for air, the uncertainties in the measurement of various parameters are observed as follows:

ΔV_m=0.1 L/min; ΔP_s =0.001bar; ΔP_d =0.0015bar; ΔT_s =0.2°C; ΔN_m =0.4 rev/s; Δm_e =0.015kg/min; Δn_e =0.12rev/min; Δt_e=0.02s; Δm_t =0.017kg/min

Substituting the above values of different measurable quantities and the corresponding uncertainties in the relevant equations, the uncertainties in the measurement of volumetric and adiabatic efficiency are calculated.

The error in the measurement of volumetric and adiabatic efficiency for air are calculated to be

$\Delta \eta_{ev}$= 0.054 for η_{ev} =0.89

$\Delta \eta_{ea}$ = 0.039 for η_{ea} = 0.5781

An error analysis has been performed for all sets of readings and the level of uncertainties is found to be of the same order. Conservative estimates of the uncertainties, which are generally applicable to all the test results, are as follows

$$\frac{\Delta\eta_{ev}}{\eta_{ev}} = \pm 6.0\%$$

and

$$\frac{\Delta\eta_{ea}}{\eta_{ea}} = \pm 7.0\%$$

6. Discussion

Theoretical and experimental studies have been conducted on a commercially available air compressor using both air and helium as working fluids. The variation of volumetric efficiency with discharge pressure for air and helium is presented in Fig 6. The variation of volumetric efficiency at higher discharge pressures is negligible. This happens because the screw compressor doesn't have any clearance volume at the end of compression process. Our result is similar to those results obtained by Osada and Fujiwara [4] and by Stosic *et al* [12]. The difference in theoretical and experimental values is attributed to be imperfect nature of ports, wall friction and other frictional losses apart from leakage loss. Variation of adiabatic efficiency with discharge pressure is estimated using the procedure described and shown in Fig 7. The nature of change of adiabatic efficiency with discharge pressure is similar for helium and air. The figure shows that there exists an optimum pressure ratio for the highest adiabatic efficiency.

The influence of interlobe clearance on the P-V diagram of a 5+6 rotor combination using air and helium as a working media is presented in Figs 8 and 9 respectively. The nature of the P-V diagram is similar to those of Ref [8, 13] for adiabatic compression. The result shows that the area of P-V diagram decreases with increase of interlobe clearance. The decrease is more severe for helium than for air. This is because of the higher decrease of mass in the compression chamber caused by the increased interlobe gas leakage at higher interlobe clearance. Helium being a low molecular weight gas can easily escape through narrow gap leading to higher leakage loss.

The influence of injected oil quantity on temperature of gas and oil is shown in Figs10 and 11 for air and helium respectively. It is observed that enhancement of oil to gas mass ratio beyond a certain limit, has little effect on temperature of the compressed gas. Most of the heat of gas compression is transferred to the oil when the discharge port opens as shown in the figures. The rise in oil temperature is relatively less due to its high specific heat capacity. Also, the rise in temperature of helium gas is relatively more than that of air. This effect is attributed to the higher specific heat ratio (γ=1.67) for helium and relatively less heat transfer coefficient value (1.4656kW/m^2K). The value of oil to gas mass ratio used in the simulation model are derived from the experimental data. This ratio is much higher for helium compared to air. The theoretical values of gas temperatures obtained during compression process (for both air and helium) are higher than the expected values. This is because it has been assumed that during compression process, the heat of compression is transferred only to oil. In reality, oil and gas are mixed and a significant fraction of the heat will be transferred to the screw rotors and the casing. In fact, the compressor system has a cooling mechanism, where the heat of compression is continuously dissipated to the environment.

The influence of interlobe clearance and rotational speed of male rotor is presented in Fig 12.The decrease of volumetric efficiency with an increase of interlobe clearance is more severe at lower rpm for helium than air as shown in figure, because of its lower molecular weight, the gas can easily escape through narrow gap. The blowhole area is inherent in the contour of the rotor. The effect of blowhole area on the estimated volumetric efficiency is presented in the Fig 13. Volumetric efficiency variation with increase in blowhole area on air is less at higher rpm, and somewhat higher for helium, the difference can largely be attributed to helium being a light gas.

7. Conclusions

A numerical model of the oil injected dual screw compressor has been developed covering both suction and compression-discharge steps to study the influence of design and operating parameters on the compressor volumetric and adiabatic efficiencies. Heat transfer coefficient between gas and oil has been determined from experimental observations in which volumetric efficiency decreases with decrease of inlet temperature. Flow coefficients have also been determined from experimentally obtained compressor efficiencies. The influence of operating and design parameters is studied and some quantitative results have been obtained to convert commercially available oil injected air screw compressor for helium compression.

Acknowledgements

The authors are grateful to the Board of Research in Nuclear Sciences (Department Atomic Energy) who sponsored and financed for this project work. The authors are thankful to the Mechanical Engineering Department, NIT, Rourkela, for providing all testing facilities and guidance.

References

[1] **Pawan, J. Singh, and Onuschak, A.D.** A comprehensive, Computerized Method for twin Screw rotor Profile generation and Analysis, Proceedings of the Purdue Compressor Technology Conference, Purdue, USA, (1984), 519-527

[2] **Pawan, J. Singh, and Patel, G.C.** A generalized performance computer program for oil flooded twin-screw compressors, Proceedings of the Purdue Compressor Technology Conference, Purdue, USA, (1984), 544-553.

[3] **Koelet, P.** Industrial Refrigeration, Principle, design and Applications, Mc Graw Hill, (1992)

[4] **Fujiwara, M., Osada, Y.** Performance analysis of oil injected screw compressor and its application, International Journal of refrigeration, (1995), Vol. 18, No 4, 220-227

[5] **Sangfors, B.** Computer Simulation of Oil injected Twin-screw compressor, Proceedings of the Purdue Compressor Technology Conference, Purdue, USA, (1984), 528-535

[6] **Pietsch, A., and Nowotny, S.** Thermodynamic calculation of a duel screw compressor based on experimentally measured values taking supercharge into account, International compressor Engineering conference, Purdue, USA, (1990), Vol-I, 44-50

[7] **Wu Huagen, Xing Ziwen, Shu Pengcheng** Theoretical and experimental study on Indicator diagram of twin screw refrigeration compressor, International journal of refrigeration, volume 27, Issue 4, June 2004, 331-338

[8] **Fujiwara, M., Kasuya, K., Matsunaga, T., Makoto, W.** Computer Modeling for performance analysis of rotary screw compressor, Proceedings of the Purdue Compressor Technology Conference, Purdue, USA, (1984), 536-543

[9] **Fujiwara, M., Mori, H., and Suwama, T.** Prediction of the oil free screw compressor performance using digital computers, Proceedings of the Purdue Compressor Technology Conference, Purdue, USA, (1974), 186-189

[10] **Robert, W. Fox., Alan T. McDonald** Introduction to Fluid Mechanics, 2nd Edition, John Wiley & Sons (1973)

[12] **Stosic, N. Smith, I.K., Kovacevic, A.** Retrofit 'N' Rotors for efficient oil flooded screw compressors, International Compressor Conference, Purdue, USA, (2000), 917-924

[11] **Ueno, K., Hunter,K.S.** Compressor efficiency definitions, www.vairex.com (May 12th, (2003)

[13] **Huagen Wu, Xueyuan Peng, Ziwen Xing, Pengcheng Shu** Experimental study on P-V Indicator diagrams of twin screw refrigeration compressor with economizer, Applied thermal engineering, volume 24, Issue 10, July 2004, 1491-1500

[14] **Taylor, R.P., Hodge, B.K., James, C.A.** Estimating Uncertainty in Thermal systems analysis and design, Applied Thermal Engineering, (1999) **1** (1) 3-17

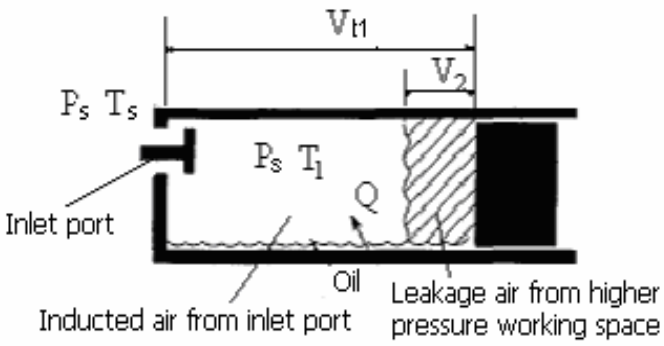

Figure 1 Model of the working chamber of an oil injected twin-screw compressor cavity at the end of the suction process [4]

Figure 2 A view of the experimental setup used to measure various operating parameters of screw compressor

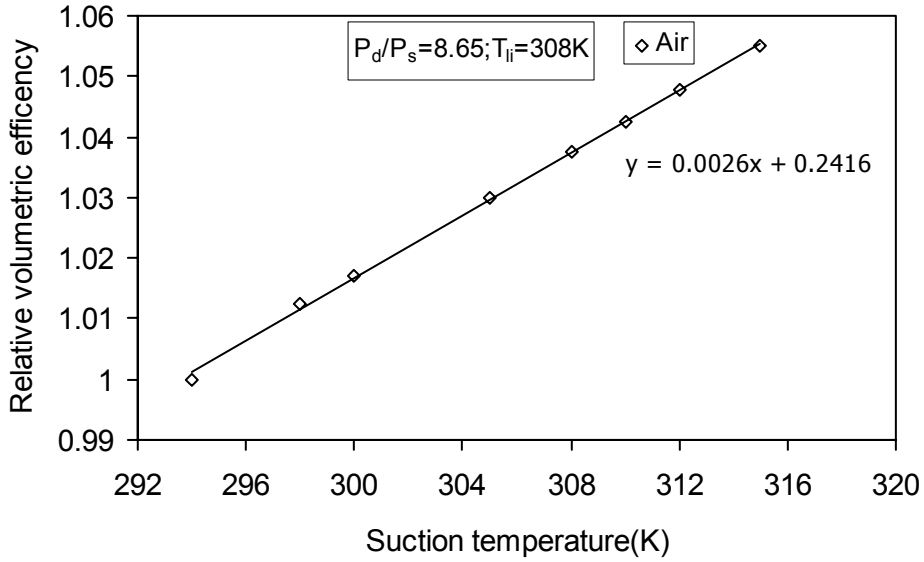

Figure 3 Experimental volumetric efficiency curve against suction temperature (efficiencies are relative to suction temperature of 294K)

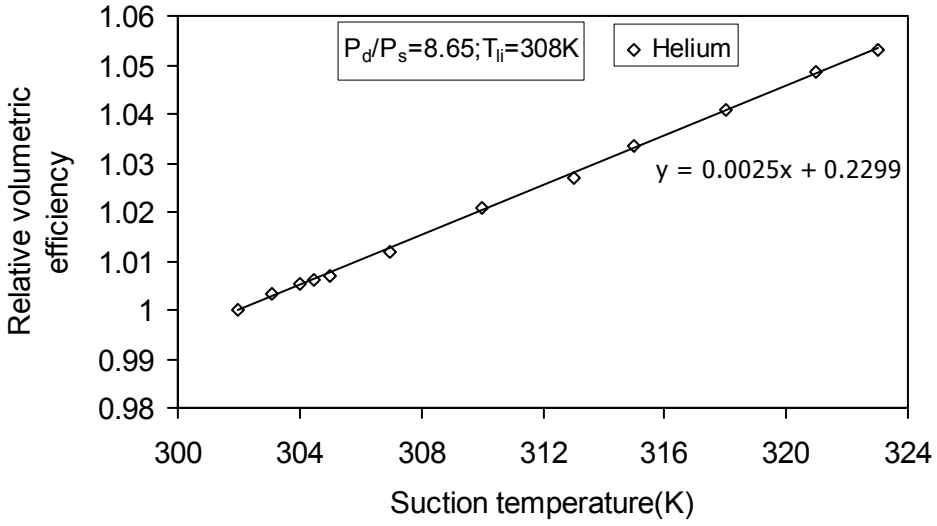

Figure 4 Experimental volumetric efficiency shown against suction temperature (efficiencies are relative to suction temperature of 302K)

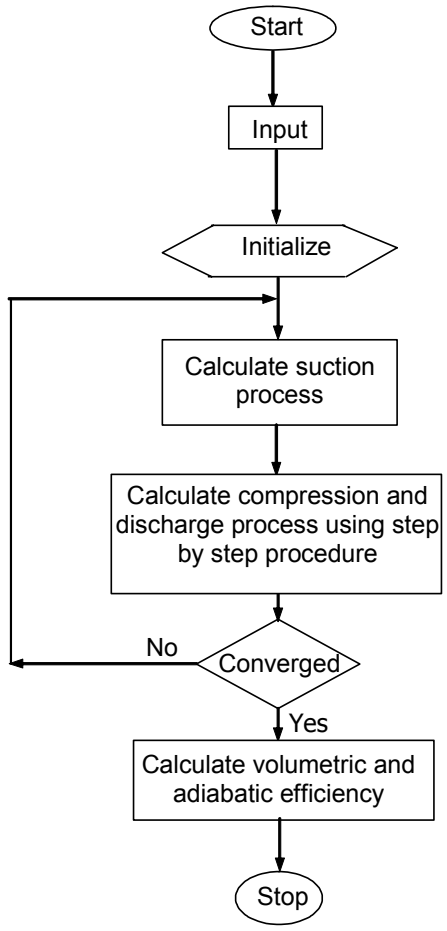

Figure 5 Flow diagram for solution of governing equations of a screw compressor

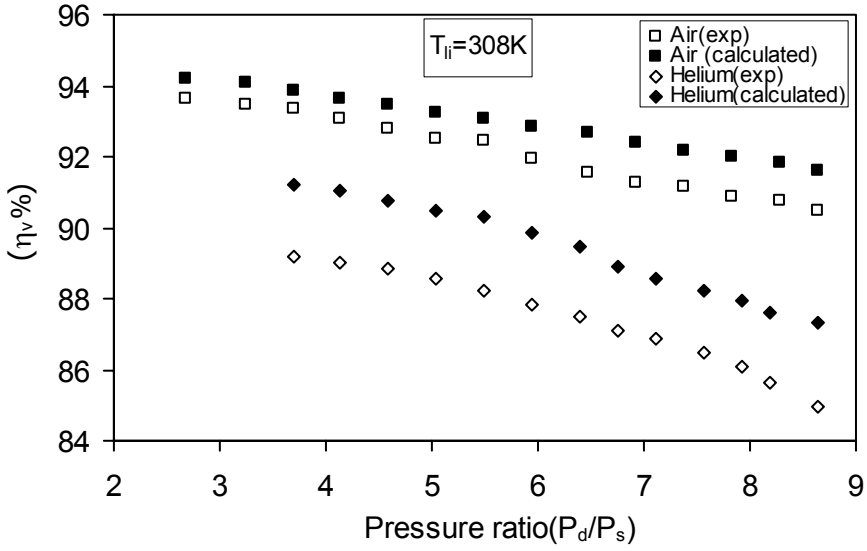

Figure 6 Variation of volumetric efficiency with discharge pressure at a fixed injected oil temperature and other inlet conditions

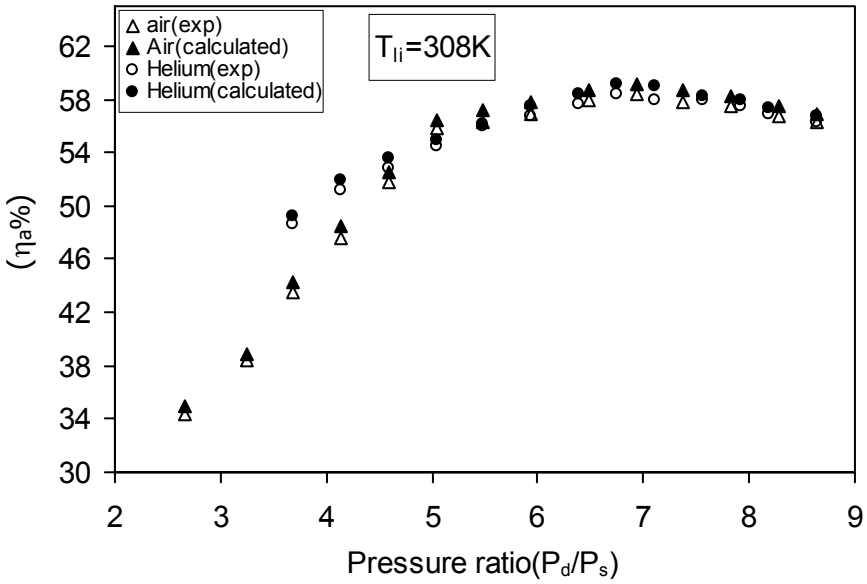

Figure 7 Variation of adiabatic efficiency with discharge pressure at constant inlet condition at a fixed injected oil temperature

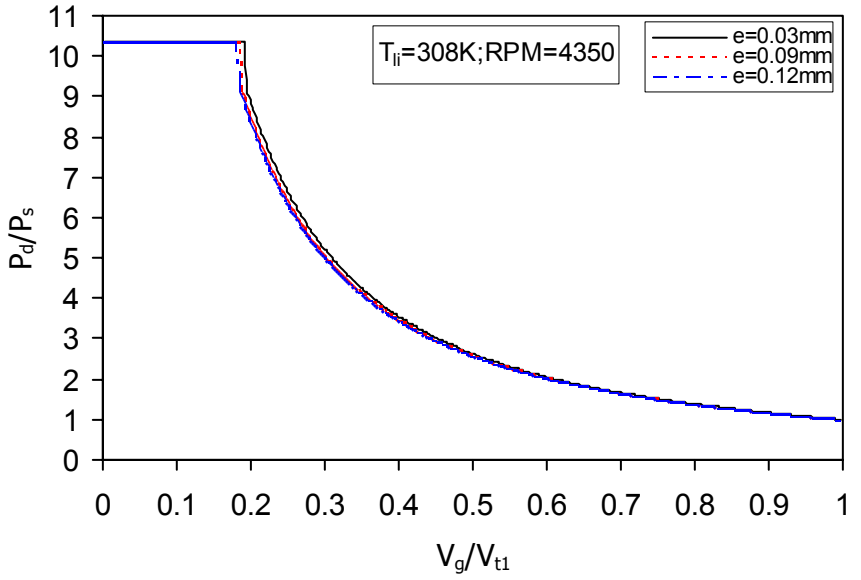

Figure 8 Effect of interlobe clearance on P-V diagram profile of air at a fixed injected oil temperature and inlet conditions

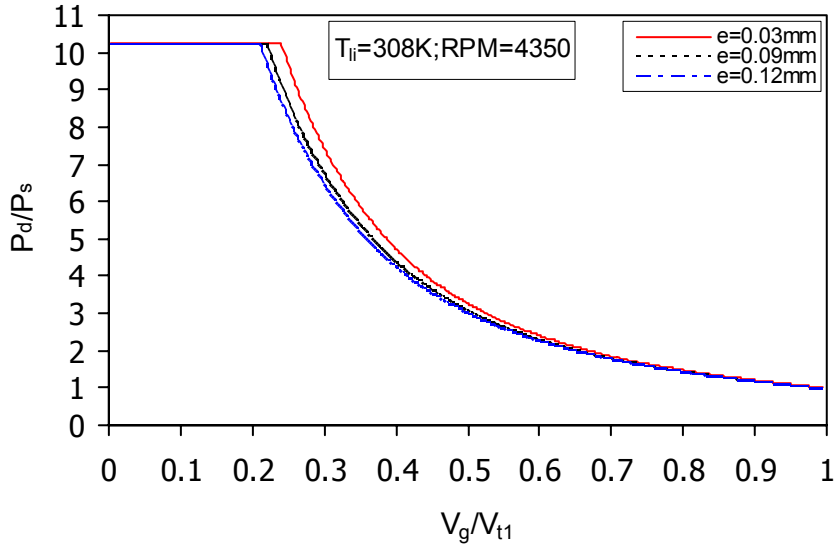

Figure 9 Effect of interlobe clearance on P-V diagram profile of helium at a fixed injected oil temperature and inlet conditions

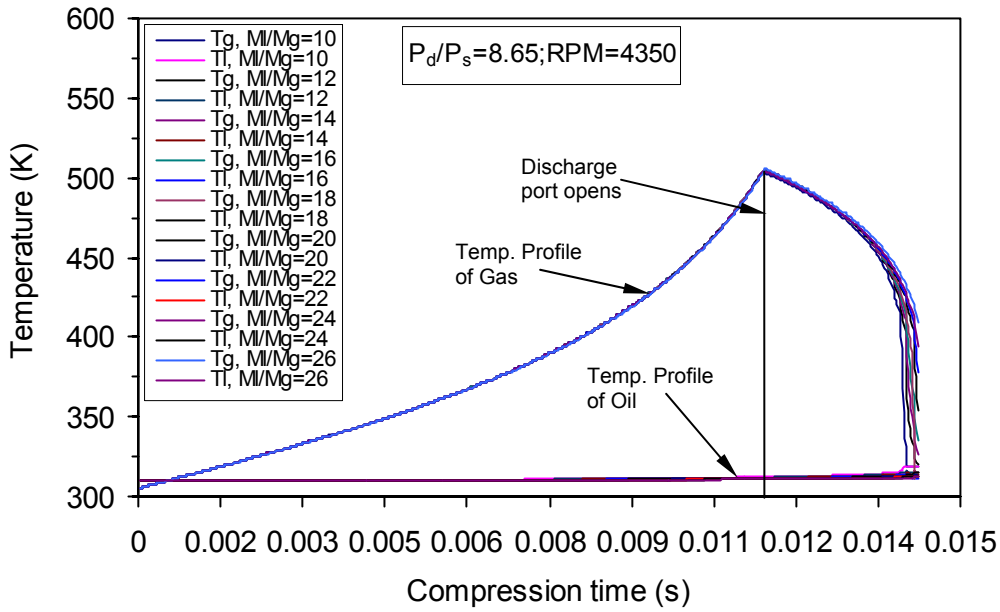

Figure 10 Variation of gas and oil temperatures during compression process at different oil to gas mass ratio and inlet conditions

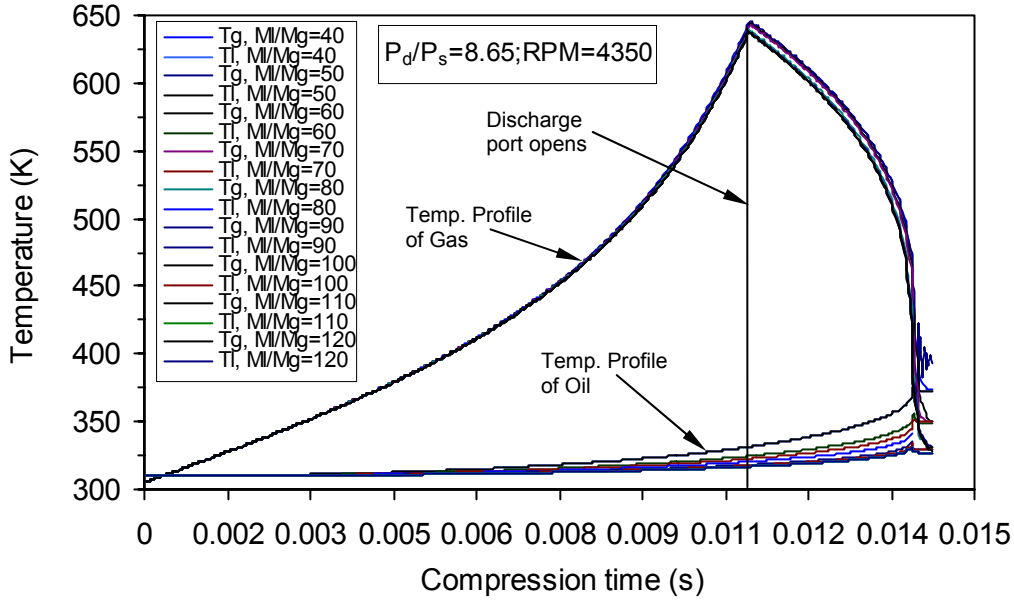

Figure 11 Variation of gas and oil temperatures during compression process at different oil to gas mass ratio of helium at a fixed pressure ratio and inlet conditions

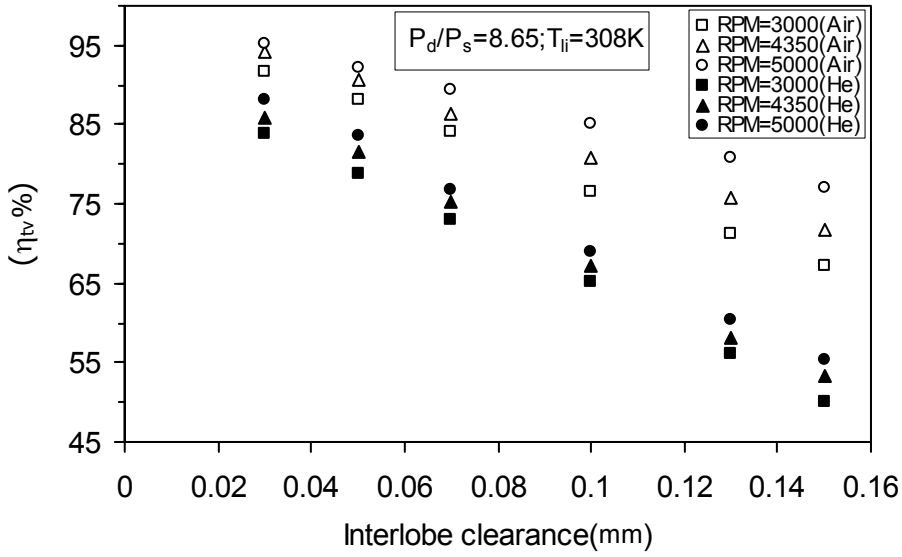

Figure 12 Influence of RPM on volumetric efficiency with interlobe clearance at a fixed injected oil temperature and inlet condition

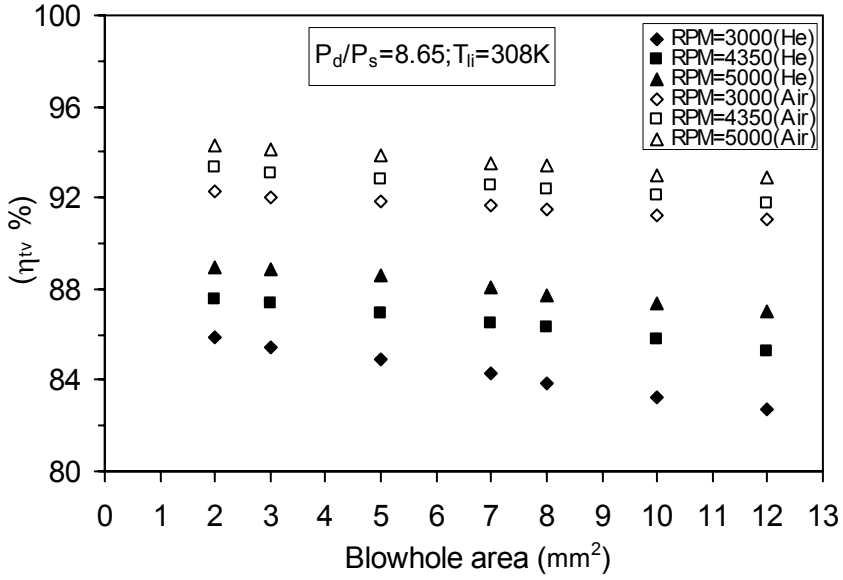

Figure 13 Effect of blowhole area on volumetric efficiency at different RPM at a fixed injected oil temperature and inlet condition

Table 1 Rotor specifications and operating conditions of prototype compressor

Profile	Sigma
Combination of number of teeth	5+6
Outer diameter of male rotor (mm)	72
Outer diameter of female rotor (mm)	54
Wrap angle (degree)	300
Rotor length (mm)	90
Theoretical volume of a pair of male and female rotor grooves (cm^3)	34.2
Built in volume ratio	5
Suction pressure (MPa)	0.1
Discharge pressure (MPa)	0.88
Rotational speed of male rotor (rpm)	4350
Supplied oil temperature (K)	308
Supplied oil rate (l/min)	23.6

Table 2 Flow coefficients and clearances at different leakage paths

Coefficient at Interlobe clearance	0.65
At lobe tip and casing bore	0.7
At leading blowhole	0.7
At lagging blowhole	0.6
Between rotor end and casing wall	0.4
Interlobe clearance (mm)	0.027
Clearance between lobe tip and casing bore(mm)	0.03
Clearance between rotor end and end plate (mm)	0.03
Leading blowhole area (mm^2)	2
Lagging blowhole area (mm^2)	2